when granules of zirconium dioxide were dropped through a nitrogen-containing plasma torch.

The nitrogen need not be in gaseous form in the system to cause the explosion. A result similar to that shown at the right of Fig. 1 also was obtained when the original squares of zirconium had been partially nitrided (by heating for 1 hour at 900°C in flowing nitrogen at 625 torr) before they were burned in pure oxygen.

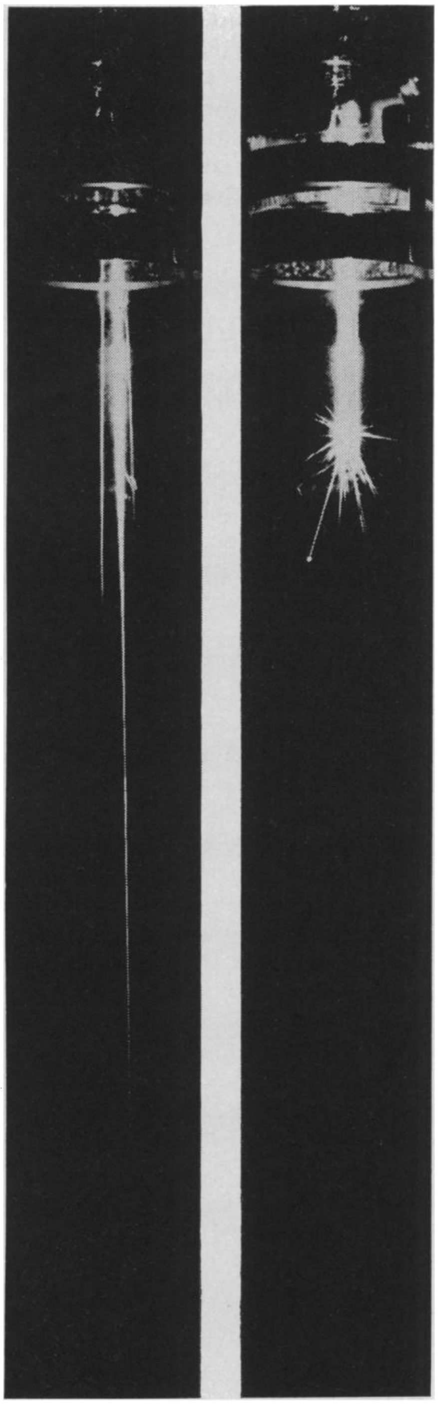

Fig. 1. The combustion of a freely falling zirconium droplet in oxygen (left) and in a mixture of 4.5 percent nitrogen and 95.5 percent oxygen (right). In each case, the droplets are burning in a 75-mm Pyrex tube containing the oxidizing gas at 625 torr flowing downward at 5.0 lit./min. Droplet diameter is 525 μ. The weak traces are reflections from the walls of the chamber.

It was reported earlier that zirconium reacts simultaneously with nitrogen and oxygen both during the low temperature oxidation of solid zirconium in air (*10*) and during the higher temperature combustion of molten zirconium droplets in air (*11*). The latter results were obtained by interrupting the combustion of the droplets at various stages by allowing them to fall into liquid argon. X-ray diffraction patterns from droplets quenched toward the end of the combustion in air (before explosion) contained strong lines arising from zirconium, zirconium nitride, zirconium dioxide and the recently characterized zirconium oxynitride, Zr_2ON_2 (*12*).

In the experiments reported here, where considerably lower concentrations of nitrogen were available to the droplets, x-ray diffraction patterns obtained in a similar manner contained strong lines arising from zirconium and zirconium dioxide, and faint lines, near the limit of detection, corresponding to the most intense lines of zirconium oxynitride.

A plausible explanation of the results cited here is that when gaseous nitrogen is present in the early stages of combustion, the molten zirconium will take up both oxygen and nitrogen to form a liquid phase that contains zirconium, oxygen, and nitrogen (similar to getter action). The same composition may also result if the zirconium is partially nitrided before being burned in pure oxygen. As the droplet burns further, its composition must eventually approach that of the thermodynamically favored zirconium dioxide so that nitrogen is subsequently liberated. When there is sufficient nitrogen present to exceed the solubility in the molten mixture, a high internal pressure of gas will form and the fragmentation will occur. Lesser concentrations of nitrogen will produce only a few inflated sacs or bulges.

This explanation is somewhat akin to that attributed to Gordon (*7*), in which the internal release of dissolved gases was considered to cause the explosions. The mechanism suggested here, however, includes but does not require the physical solution of gases in the metal before ignition. If there is insufficient gas in the metal before combustion, explosions may still occur, but now as a result of gas taken up during the initial stages of the burning reaction.

L. S. NELSON

Sandia Laboratory,
Albuquerque, New Mexico

References and Notes

1. D. A. Gordon, *Solid Propellant Rocket Research* (Academic Press, New York, 1960), vol. 1, p. 271.
2. L. S. Nelson and N. L. Richardson, *J. Phys. Chem.* **68**, 1268 (1964).
3. G. Tschorn, *Spark Atlas of Steels* (Macmillan, New York, 1963).
4. R. Friedman and A. Maček, *Combust. Flame* **6**, 9 (1962).
5. ———, in *Ninth Symposium (International) on Combustion* (Academic Press, New York, 1963), p. 703.
6. J. L. Beal, W. R. Brown, F. A. Vassalo, Fall 1964 Meeting, Western States Section, The Combustion Institute, Salt Lake City, Utah, Preprints, Paper No. 64–24.
7. Attributed to D. A. Gordon by I. Glassman, in *Ninth Symposium (International) on Combustion* (Academic Press, New York, 1963), p. 709.
8. J. Hunger and O. Werner, *Arch. Eisenhuettenw.* **23**, 277 (1952).
9. H. Meyer, *Ber. Deut. Keram. Ges.* **41**, 112 (1964).
10. C. A. Phalnikar and W. M. Baldwin, Jr., *Am. Soc. Testing Mater. Proc.* **51**, 1038 (1951).
11. L. S. Nelson, Fall 1964 Meeting, Western States Section, The Combustion Institute, Salt Lake City, Utah, Preprints, Paper No. 64–23, in press.
12. J. C. Gilles, *Bull. Soc. Chim. France* **1962**, 2118 (1962).
13. I thank N. L. Richardson for helping with the experiments, and E. J. Graeber for performing the x-ray diffraction studies. Supported by the AEC.

12 April 1965

Activation Energy of Direct-Current Electrical Conductivity of Ice with HF and NH_3 Added

Abstract. *The activation energies of ice with varying amounts of impurities added were investigated with sintered platinum electrodes. For both types of impurities the activation energy was minimum at a concentration of* 10^{-4}M. *The experimental arrangement and possible reasons for the existence of a minimum in activation energy are discussed.*

The activation energy of the d-c electrical conductivity in pure ice has been investigated by many authors (*1, 2*). There seems to be some disagreement about the values of the activation energy owing to difficulties in the interpretation of the data and possible sources of error, as well as establishment of a good ohmic contact with the sample substance. The error that is hardest to identify stems

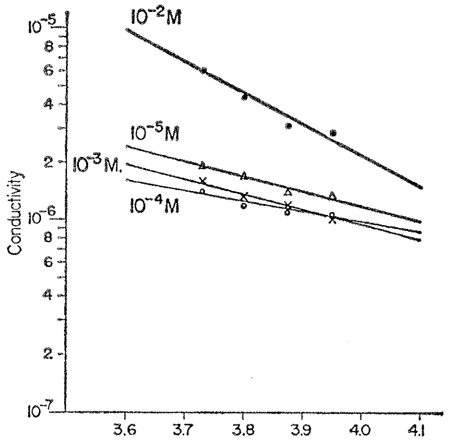

Fig. 1. Conductivity (ohm^{-1} cm^{-1}) plotted against temperature for various molar concentrations of HF.

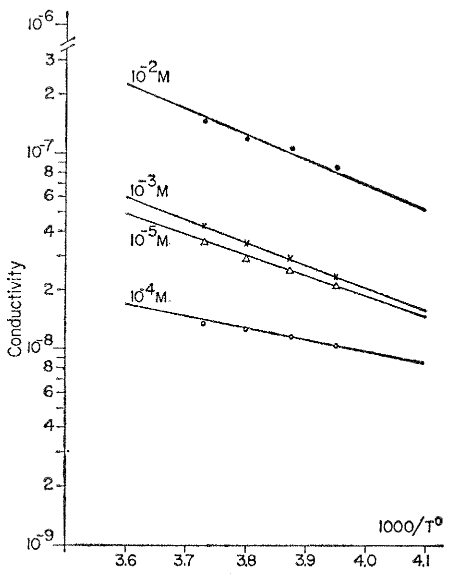

Fig. 2. Conductivity (ohm^{-1} cm^{-1}) plotted against temperature for various molar concentrations of NH_3.

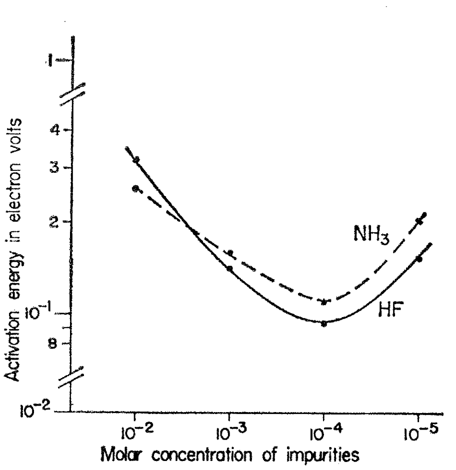

Fig. 3. Activation energy as a function of the concentration of impurities (HF and NH_3).

from the difficulty of growing very pure, single crystals of ice. Since many of the uncertainties in a study of pure ice result from measurements that are very susceptible to errors due to the possible presence of small amounts of impurities, valuable information can be obtained from an investigation of impure (doped) ice.

To arrive at a theoretical analysis of the mechanism of proton transport in ice [analogous to the basic theory of electronic semiconductors (*3*)], it is necessary to investigate the d-c conductivity of ice doped with "hydroxide" and "hydronium" ions at varying concentrations and at several temperatures. A set of such data for doped ice is not as yet available owing to the above-mentioned difficulty of obtaining reproducible results; in the case of doped samples, this difficulty consists mainly in the measurement of a time-dependent current (non-ohmic contact) caused by electrode polarization and space-charge effects.

The first obscuring effect—electrode polarization—can be somewhat alleviated by the use of "sandwich" electrodes, a method developed in studies of electronic semiconductors and sometimes adapted for ice studies (*4, 5*). In our study, as a suitable ohmic contact we selected sintered porous platinum disks with a porosity of 35 percent (Engelhard Industries, Inc.). The electrodes were soaked in solutions of HF or NH_3 at concentrations 100 times those of the actual samples. This method proved unsuitable in the case of pure ice samples because there is no definite basic reference concentration for this case, and the pure ice is very sensitive to the impurity diffusion from the porous electrodes.

The second effect—space-charge accumulation—leads to considerable changes of the potential distribution in the ice sample and to a time-dependent current. This effect seems to be due mainly to dissolved air and movement of grain boundaries of the crystals. The crystals were allowed to age for 1 day before measurement, most major imperfections in the grain structure being thereby removed. In order to check the internal field distribution of the aged ice samples, five equally spaced platinum probes (0.005 by 0.08 cm) were frozen with the samples. The samples used for the investigation of internal field were of cylindrical shape (3 cm in diameter by 7 cm). The internal field distribution was measured by a Keithley differential voltmeter model 660, and the electric field varied linearly with distance between the electrodes. The aged samples were much more stable in linear potential distribution, whereas samples which had not been aged showed considerable space charge accumulation and led to nonlinear potential distribution.

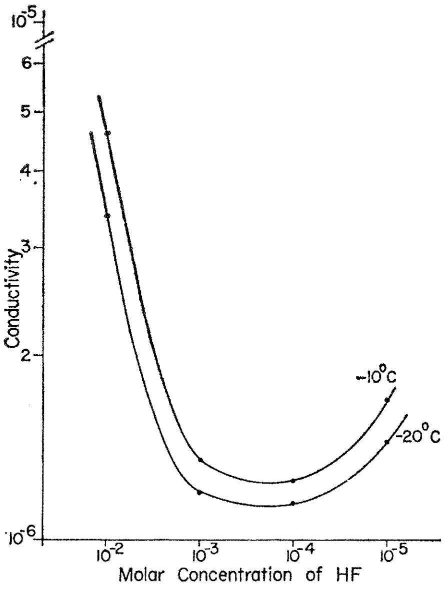

Fig. 4. Conductivity (ohm^{-1} cm^{-1}) plotted against HF concentration.

Solutions of HF and NH_3 were prepared with distilled and demineralized water. The ice samples were grown on a platinum disk fitted into a copper block at an average rate of 0.5 mm per minute. The samples used for the conductivity were of cylindrical shape

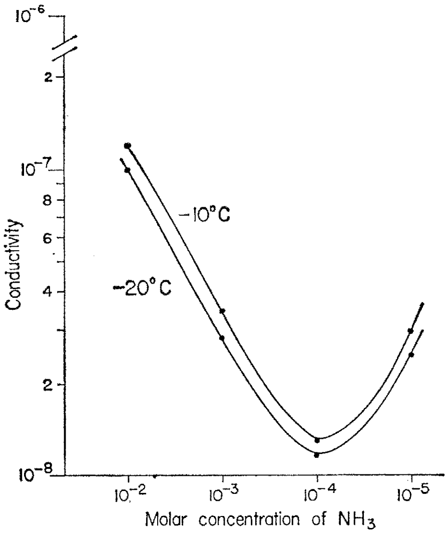

Fig. 5. Conductivity (ohm^{-1} cm^{-1}) plotted against NH_3 concentration.

(1.27 cm in diameter by 0.623 cm). Experiments were carried out between −5° and −20°C. After the ice crystal was grown, the porous electrode was attached by pressure, and the sample was aged for 30 hours. Currents were measured with a Hewlett-Packard Model 425 A microammeter and a Varian recorder in order to observe time dependence of the current. Most measurements were nearly constant with time; in those cases where a sudden change appeared only the instantaneous value of current at the first application of the electric field was used, since the discontinuity in the reading seemed to stem from the appearance of cracks due to thermal shock of the sample by ohmic heating. A change in the temperature of the sample due to resistive heating was precluded by applying the electric field for 30 seconds only after an intermittent period of 90 seconds.

The changes in conductivity at different temperatures with different concentrations of HF and NH_3 (Figs. 1 and 2) were obtained from the recorded currents at electric fields of 10, 50, 100, and 200 volts and at two polarities. The readings were taken at −5°, −10°, −15°, and −20°C, maintained accurately by submerging the samples into a Wilkens-Anderson Lo-Temp bath. The average value was used for the straight-line approximation. In almost all the experiments the currents varied linearly with the applied electric field.

Analysis of the data showed that the conductivity (σ) of the sample follows the relation of a typical semiconductor:

$$\sigma = \sigma_0 \exp(-E/kT).$$

The activation energy E was calculated with this expression, and the data are listed in Table 1. The minimum of the activation energy at $10^{-4}M$ concentration of impurities (Fig. 3) corresponds to the critical concentration at which the polarization mechanism responsible for the dielectric constant changes abruptly (*5*).

Some authors (*6*) have found a similar change in activation energy with concentration of impurities in the doped ice. The evidence now supports the conclusion that lower activation energies are associated with higher impurity content within the region of less than $10^{-4}M$ impurity concentration. The activation energy of d-c conductivity in pure ice is reported to lie between 0.5 and 1.2 ev (*1*, *2*). Our data also justify this point of view.

Table 1. Activation energy (E) of doped ice conductivity.

Concentration (M)	E (HF) (ev)	E (NH_3) (ev)
10^{-2}	0.321	0.259
10^{-3}	.143	.159
10^{-4}	.094	.111
10^{-5}	.154	.203

The d-c conductivity in doped ice is believed to require proton transfer through the hydrogen bond by tunneling and by the orientational motion of water molecules to maintain the favorable path for further transfer of protons (*5*). Hence the activation energy includes the proton tunneling energy and the water molecule's rotational energy [with the aid of double (D) and vacant (L) defects] as well as the dissociation energy of the impurity molecules. Because of the many processes involved it is not yet possible to determine which portion of the energy contributes to the change in activation energy with impurity concentration. The change in potential curves for protons in the hydrogen bond of O — F and O — N from that in O — O bonds (*7*) together with an analysis of the rotational mechanism of D and L defects may lead to the explanation of the curves represented in Fig. 3.

At concentrations higher than $10^{-4}M$ the rate of the proton transport mechanism may be controlled by the rate of rotation of the water molecules. As the impurity concentration increases, the number of D or L defects also increases, and higher activation energy results. This trend may exist because the number of rotations of the water molecule required to produce a favorable proton path increases with concentration of impurities. As the concentration is lowered below $10^{-4}M$, the rate-determining factor will be the proton-tunneling process because the number of defects that undergo rotation is reduced eventually to a negligible amount. The proton tunneling seems more difficult as the numbers of impurities decrease. The proton tunneling becomes harder as the structure becomes more nearly perfect, which seems to be due to the higher proton tunneling energy through O — O hydrogen bonds as compared to that of O — N or O — F bonds.

Qualitatively, the lowest activation energy at $10^{-4}M$ impurity concentration may be interpreted as a change in the rate-determining step from orientational motion to proton tunneling through the hydrogen bonds.

Figures 4 and 5 show the change in conductivity of the samples at −10° and −20°C as a function of the amount of doping with HF and NH_3, respectively. These figures are obtained from Figs. 1 and 2. The results indicate that the d-c conductivity of doped ice at constant temperature is not directly proportional to the concentration of impurities. Since the conductivity is a function of both impurity content and charge-carrier mobility, the mobility might cause the nonlinear change in conductivity with the concentration of impurities (Figs. 4 and 5).

Since the mobility depends upon scattering, it is a function of both the temperature and the density of impurity. Study of the temperature dependence may be based on the existing theory of semiconductors, such as impurity scattering and lattice scattering. Impurity scattering is more important than lattice scattering in our study because of the higher mobility at higher temperatures. The phenomenon of a change in ice conductivity with temperature by different types of scattering was observed by some investigators (*2*).

The mobility dependence upon density of impurity is not clear. Unfortunately, conductivity in the region where the impurity content is less than $10^{-5}M$ cannot be measured accurately as yet. However, there should exist an inversion point to decrease the conductivity (Figs. 4 and 5) such that it can be extrapolated to the pure-ice conductivity of 10^{-8} to 10^{-9} ohm^{-1} cm^{-1} which is supported by some investigators (*3*). In the electronic theory of semiconductors (*8*), the mobility increases as the impurities decrease and reaches a saturation value at a certain density of impurity. From this point of view, the possible inversion point can be interpreted as the saturation level of mobility, and the conductivity will be a function of only impurity content between inversion point concentration and pure ice.

S. Y. Chai
P. O. Vogelhut
Department of Electrical Engineering,
Electronics Research Laboratory,
University of California, Berkeley

References and Notes

1. R. S. Bradley, *Trans. Faraday Soc.* **53**, 687 (1957).
2. F. Heinmets and R. Blum, *ibid.* **59**, 1141 (1963).

→ M. Eigen and L. De Maeyer, *Proc. Roy. Soc. London Ser. A* **247**, 505 (1958).

4. G. W. Gross, *Science* **138**, 520 (1962).
5. H. Gränicher, C. Jaccard, P. Scherrer, A. Steinemann, *Discussions Faraday Soc.* **23**, 50 (1957).
6. L. Levi and L. Lubart, *J. Chim. Phys.* **58**, 863 (1961).
7. E. R. Lippincott and R. Schroeder, *J. Chem. Phys.* **23**, 1099 (1955).
8. E. M. Conwell, *Phys. Rev.* **96**, 1281 (1958).
9. Supported by ONR, contract Nonr-222(92).

15 March 1965

Ocean-Bottom Topography: The Divide between the Sohm and Hatteras Abyssal Plains

Abstract. *A compilation of precision echo soundings has delineated the complex topography between the Sohm and Hatteras abyssal plains off the Atlantic coast of the United States. At present the divide between the two plains is a broad, flat area about 4950 meters deep; however, the configuration of channels and depressions suggests spillage of turbidity currents from the Sohm Plain into the Hatteras Plain and a shifting of the divide toward the northeast. Hudson Canyon terminates in the divide area and has probably fed sediment into both plains.*

A recent compilation of precision echo soundings off the East Coast of the United States has delineated reasonably well the area of complex topography between the Sohm and Hatteras abyssal plains (Fig. 1). Sounding lines used in compiling the topographic map (Fig. 2) are entirely those of Woods Hole Oceanographic Institution ships. They have a depth accuracy of within 10 meters, although in some instances the position of the lines may be in error by as much as 18 kilometers. The map is contoured in meters from original data compiled in fathoms and corrected for the velocity of sound in water.

Sohm Abyssal Plain extends eastward from the base of the continental rise and generally occupies the deep basin between Canada and Bermuda. Its western end is partially ponded by the New England Seamounts and consequently exhibits very gentle gradients, as shown in the northeast corner of Fig. 2. It is now generally recognized that the abyssal plains are formed largely of terrigenous or land-derived sediment transported to the ocean floor by turbidity currents. The sediment in the Sohm Abyssal Plain appears to be derived mainly through the submarine canyons along the slope off New England.

The Hatteras Abyssal Plain occupies the deep basin between southeastern United States and Bermuda. The plain deepens gradually to the south, indicating that the principal source of the sediment deposited is at the north. The northernmost end of the Hatteras Plain terminates in a series of deep-sea channels shown in the southwest corner of the map area.

The largest submarine canyon on the East Coast is Hudson Canyon. During the Pleistocene epoch, when the Hudson River was a major outlet for the Great Lakes and the shore line was at the outer edge of the shelf, the Hudson Canyon was probably a major channel for turbidity currents. At present it appears to be inactive. The canyon has been traced as a well-defined gorge down the continental slope and across the continental rise. Originally it was thought to terminate by merging with the western end of the Sohm Abyssal Plain in the vicinity of Caryn Seamount (*1*). However, recent echo soundings indicate that a series of shallow distributaries radiate from the canyon on a broad apron called the Hudson submarine fan, and longitudinal profiles of the canyon and adjacent sea floor show that the shortest path with the steepest gradient is now south, along the western edge of the fan, into the north end of the Hatteras Abyssal Plain.

At present the actual divide between Sohm and Hatteras abyssal plains is the broad flat area at 37°N, 65°30′W defined by the 4950-meter contour lines. Turbidity currents flowing down the continental rise in this area could flow east into the Sohm Plain or southwest through a broad channel into the Hatteras Plain. It is unlikely that they flow southeast because of a gentle rise in the bottom beyond which are unfilled depressions. The possibility that turbidity currents spilled from the Sohm Plain into the Hatteras Plain in a number of places is suggested by the relief of the low ridge at the south side of the Sohm Plain, extending over 200 miles east from the divide. Turbidity-current floods on the Sohm Plain overflowing into the depression area to the south might then flow on into the Hatteras Plain through the gap at 34°30′N, 64°W.

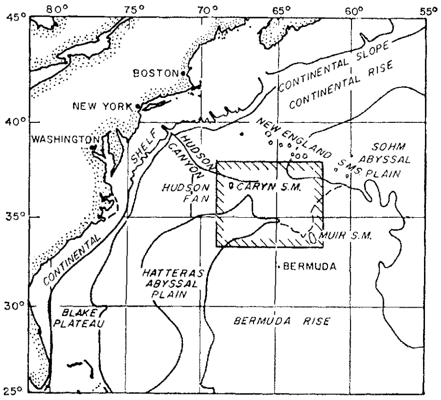

Fig. 1. Position of the area of complex topography between the Hatteras and Sohm abyssal plains. The dashed line represents the seaward limit of deposition of terrigenous sediment between the two plains.

The origin of the depressions in the central part of the map area is uncertain. Three explanations for them are (i) recent tectonic features; (ii) areas of nondeposition, out of reach of turbidity currents; and (iii) scour depressions formed by the actual removal of material by turbidity currents. Perusal of the chart gives the impression that the larger depressions owe their existence to nondeposition: these depressions lie in the shadow zone of the low ridge to the north and west and are thus protected from direct filling by turbidity currents. However, some of the smaller, closed depressions appear to be associated with the gap that connects the large depressions with the northern end of the Hatteras Plain (34°30′N, 64° to 65°W) and they may be partly scoured out by turbidity currents in the gap. The echo-sounding records show clearly that these smaller depressions do not join to form a continuous, well-defined channel through the gap but are part of a zone of relatively rough topography. These depressions are often associated with hills that could be natural levees.

The topography of the ocean floor off the northeast coast of the United States reflects the general features of a vast basin of sedimentation. To be consistent with this regional picture the topography portrayed in Fig. 2 must be interpreted as primarily sedimentary in origin. Large percentages of sand and silt in available cores (*2*), subbottom echoes, and minor topographic features indicative of small channels and natural levees are evid-